J Mater Sci: Mater Electron **(2024) 35:1363**

Improvement of the electrical properties of textured BNKT-modified (K, Na)NbO_3 lead-free ceramics in the broad operating temperature range

Le Tran Uyen Tu[1], Le Dai Vuong[2,*], Ngo Xuan Cuong[2], Nguyen Quang Lich[2], Nguyen Dang Nhat[2], Le Dinh Hieu[2], Vo Thi Thanh Kieu[3], Trinh Ngoc Dat[4], and Pai-Chun Wei[5]

[1] *University of Sciences, Hue University, Hue, Vietnam*
[2] *School of Engineering and Technology, Hue University, Hue, Vietnam*
[3] *Hue Industrial College, Hue, Vietnam*
[4] *University of Science and Education, University of Danang, Da Nang, Vietnam*
[5] *Department of Materials Science and Engineering, National Cheng Kung University, Tainan 70101, Taiwan*

Received: 15 April 2024
Accepted: 28 June 2024
Published online: 8 July 2024

ABSTRACT

In this study, the improvement in the electrical properties of textured BNKT-modified (K, Na)NbO_3 ceramics was extensively investigated across a broad, high operating temperature range. Herein, the two crucial issues of phase transitions and microstructure improvement of BNKT-modified (K, Na)NbO_3 ceramics were discussed utilizing the crystal orientation technique. Additionally, we have verified the existence of phase transition temperatures for the *R–O* phase ($T_{R–O}$), *O–T* phase ($T_{O–T}$), and *T–C* phase (T_C). This is based on the research on the temperature-dependent characteristics of the random and textured BNKT-modified (K, Na)NbO_3 lead-free ceramics in the temperature range of −100 to 420 °C. The experimental results revealed a significant improvement in the electrical properties of ceramics, which was attributed to the strategy of shifting $T_{R–O}$ and $T_{O–T}$ phase transitions to near *RT*, forming *R–O–T* phase boundaries. Besides, the textured KNLNS-BNKT ceramic with 82% grain orientation demonstrated better dielectric, piezoelectric, and ferroelectric properties compared to those randomly fabricated by the traditional ceramic method (the ε_r of 1223, the P_r of 13.5 μC/cm^2, the d_{33} of 245 pC/N, and the k_p of 0.4 increased by 11.7%, 8%, 25%, and 11%, respectively). Moreover, the normalized strain (d_{33}*) achieved a maximum value of 495 pm/V at 50 °C under an electric field of 24 kV/cm.

Address correspondence to E-mail: ldvuong@hueuni.edu.vn

https://doi.org/10.1007/s10854-024-13120-3

1 Introduction

For decades, scientists have acknowledged the significance of ceramic systems based on the application of lead zirconate titanate, $Pb(Zr,Ti)O_3$ (PZT), in numerous devices like sensor probes and ultrasonic transducers, owing to their remarkable ferroelectric and piezoelectric properties [1–4]. However, the synthesis and use of lead-containing ceramics are disadvantageous for the environment due to the high toxicity of PbO, which constitutes a large proportion of the original mixture [3, 5]. Therefore, it is vital to develop lead-free ceramics with good ferroelectric and piezoelectric properties that can replace lead-based ceramics. Recent studies have highlighted the superiority of the KNN-based ceramic system in terms of its good piezoelectric effect and high Curie temperature (the tetragonal-to-quasi cubic phase transition, T_C ~ 420 °C) [6].

It is known that a novel strategy has been developed to construct a new rhombohedral (R)—orthorhombic (O)—tetragonal (T) phase boundary can be adjusted via simple doping methods using (Sb, Li, Ta) or complex doping methods using $Bi_{0.5}(Na_xK_{1-x})TiO_3$, $Bi_{0.5}(Na_xK_{1-x})ZrO_3$, $Bi_{0.5}K_{0.5})HfO_3$, $Na_{0.5}HfO_3$, $SrZrO_3$, $CaZrO_3$, $BaZrO_3$, and $BaTiO_3$) to the KNN-based ceramics to tailor rhombohedral–orthorhombic phase transition temperature (T_{R-O}) and orthorhombic–tetragonal phase transition temperature (T_{O-T}) to room temperature simultaneously, which improving their piezoelectric properties [5, 6]. Specifically, the modifications of ions at the B-site of KNN ceramics can decrease the T_{O-T} while simultaneously increasing the T_{R-O}. These modifications lead to improved electrical properties of ceramics that meet the requirements of practical applications. As per our recent study, a multi-phase coexistence with piezoelectric properties was achieved by combining the solid mixture of KNLNS and BNKT [5]. The report reveals that the best electrical properties of KNLNS-BNKT ceramics are obtained at a content of 0.02 mol BNKT, yielding the following values: $k_p = 0.35$, $\varepsilon_r = 1287$, $d_{33} = 217$ pC/N, $Q_m = 108$, and $P_r = 15.3$ μC/cm^2 [5]. According to the recent research by Feng et al. [7], 0.98KNLNS-0.02BZ ceramics exhibit both T_{R-O} and T_{O-T} as an effective means to improve the electrocaloric effect in the ceramics. There have been several prior studies on the phase evolution of KNN-based ceramics materials from orthorhombic phase → rhombohedral-orthorhombic-tetragonal → rhombohedral-tetragonal → rhombohedral phase with impurities BNKZ and BNKT or Sb.

Furthermore, orientation control techniques have been extensively utilized to improve the electrical properties of (K, Na)NbO_3 lead-free ceramics, which have undergone significant recent advancements. According to Li et al. [8], the textured $0.96[(K_{0.5}Na_{0.5})(Nb_{0.95}Sb_{0.05})O_3]$–$0.01CaZrO_3$–$0.03(Bi_{0.5}K_{0.5})HfO_3$ ceramics synthesized using crystal orientation techniques showcase the best piezoelectric properties currently available with d_{33} of 700 pC/N and k_p of 0.76. Besides, Saito et al. employed orientation techniques and reported a large d_{33} of 416 pC/N and a high k_p of 0.61) in $(K_{0.44}Na_{0.52}Li_{0.04})(Nb_{0.86}Ta_{0.10}Sb_{0.04})O_3$ ceramics at the morphological phase boundary [9]. Therefore, in this study, we expect to discover new characteristics of textured BNKT-modified (K, Na)NbO_3 lead-free ceramics in the wide temperature range of −100–420 °C. Additionally, this study aims to address the increasing electrical properties of KNLNS–BNKT lead-free ceramics through multi-phase coexistence with crystal orientation.

2 Experimental section

For the experiment, textured $0.98(K_{0.48}Na_{0.48}Li_{0.04})(Nb_{0.95}Sb_{0.05})O_3$–$0.02Bi_{0.5}(Na_{0.4}K_{0.1})TiO_3$ lead-free ceramics was prepared via the template grain growth method utilizing platelet-like $NaNbO_3$ templates. The synthesis of ceramics through this method involves the following three stages: (i) preparation of the $NaNbO_3$ templates (Fig. 1a); (ii) preparation of the KNLNS-BNKT powder (Fig. 2a); and (iii) preparation of oriented KNLNS-BNKT ceramics (Fig. 2b).

The starting materials in the first stage include Na_2CO_3 (99.5%), Nb_2O_5 (99.5%), and Bi_2O_3 (99.5%), which were weighed according to the formula of $Bi_{2.5}Na_{3.5}Nb_5O_{18}$. Subsequently, they were milled and reacted at 1050 °C for 2.5 h (Fig. 1a). Here, the $NaNbO_3$ templates with a high aspect ratio were obtained through the topochemical microcrystal conversion method, wherein $Bi_{2.5}Na_{3.5}Nb_5O_{18}$ was converted to $NaNbO_3$ in NaCl molten salt at 950 °C for 2 h (see Fig. 1b, c). This is represented in the following equation (1):

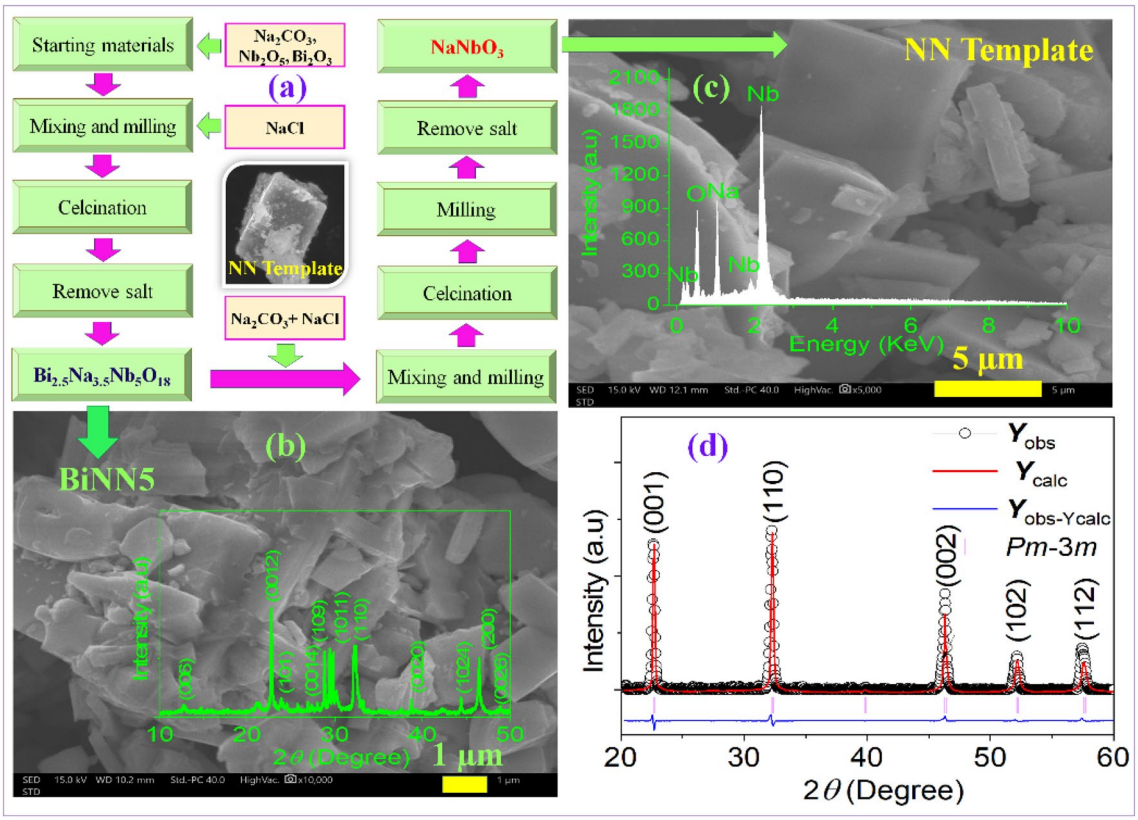

Fig. 1 **a** Fabrication diagram; **b** characteristics of $Bi_{2.5}Na_{3.5}Nb_5O_{18}$ precursor particles; and **c**, **d** characteristics of $NaNbO_3$ templates

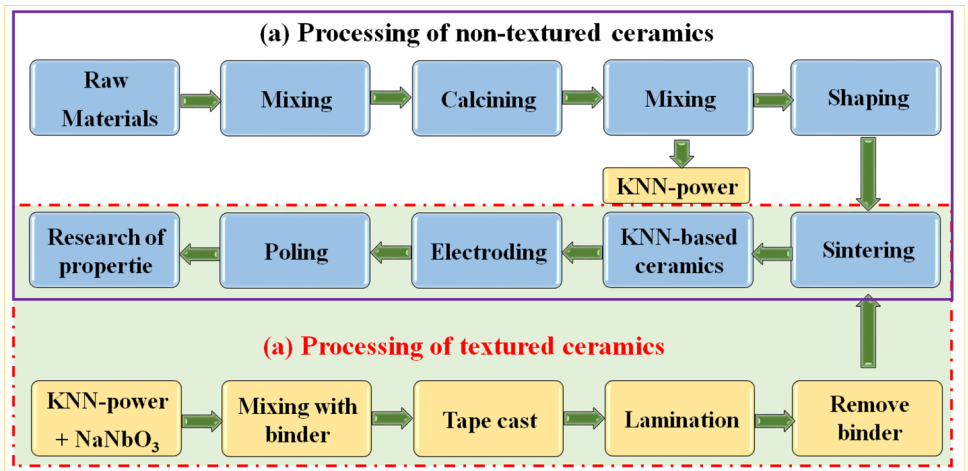

Fig. 2 Synthesis process of KNLNS–BNKT ceramics

$$4Bi_{25}Na_{3.5}Nb_5O_{18} + 3Na_2CO_3 \xrightarrow{\text{Nacl}} 20NaNbO_3 + 5Bi_2O_3 + 3CO_2. \quad (1)$$

Figure 2a depicts the second stage, which presents the synthesis process of KNLNS–BNKT powder. The starting materials in this stage, which are in the form of metal oxides and salt carbonates with purity above 99.0%, include Na_2CO_3, K_2CO_3, Nb_2O_5, Sb_2O_3, Li_2CO_3, Bi_2O_3, and TiO_2. This mixture was milled together for 20 h using a planetary ball mill in an ethanol environment. Subsequently, this mixture was dried and

calcined at 850 °C for 2 h, forming the compound KNLNS–BNKT.

In the final stage, as illustrated in Fig. 2b, the KNLNS–BNKT powders, $NaNbO_3$ templates, and binder PVA solvent were mixed for 1 h to form tape-casting slurries. They were mixed in the KNLNS–BNKT + %mol $NaNbO_3$ and binder of 30 wt% and then stirred magnetically for 30 min to create a homogeneous suspension solution for tape casting. After naturally drying the film for 12 h, it was cut into a circular shape with a diameter of 12 mm, laminated into a multilayer sheet (50–60 membrane layers), and subjected to a pressure of 3 tons/cm^2 for 5 min. The laminated green compacts were removed from organic additives at 550 °C for 1 h and sintered using a two-step sintering process [3] (T_1 = 1150 °C for 5 min, followed by T_2 = 1050 °C for 4 h) to ensure adequate epitaxial growth of grains. This technique is considered to be more effective in increasing the density and microstructure than the one-step sintering process [10].

The crystalline phase of the sintered KNLNS–BNKT ceramics was examined through X-ray diffraction (XRD, D8 Advance), and the surface morphology was determined through the images of scanning electron microscopy (SEM, Hitachi S-4800). The presence of the phase structures and electron density distributions was also confirmed by the Rietveld refinement of XRD data for $NaNbO_3$ templates. To discover the existence of the phase transition temperatures T_{R-O}, T_{O-T}, and T_C, the temperature-dependent dielectric properties were measured using an LCR meter (HIOKI 3532) in the temperature range of −100–420 °C. Moreover, Raman scattering spectra were recorded using a Raman spectrometer (Jobin–Yvon Inc., Paris, France). Energy-dispersive spectra (EDS) and surface morphologies were measured using a Hitachi S-3400 N scanning electron microscope with an EDS system from Thermo Noran.

To determine the texturing degrees of the ceramic, the Lotgering factor (f), which is the intensity fraction of preferred crystallographic orientation by Eqs. (2) [11], and X-ray diffraction data were recorded over a 2θ range of 20º to 60º.

$$f = \frac{P - P_o}{1 - P_o}, \tag{2}$$

where $P = \frac{\sum I(00l)}{\sum I(hkl)}, P_o = \frac{\sum I(00l)}{\sum I(hkl)}$, and $\sum I(00l)$ and $\sum I(hkl)$ are the sums of the intensities of the (00 l) and (hkl) reflections, respectively; further, P_o is the value of P for a random sample used in the study. The ferroelectric hysteresis loops (P–E) were measured by the Sawyer–Tower method and the strain curves (S–E) of ceramics were tested by a ferroelectric test system (aixACCT TF-analyzer 1000). Following the poling of the KNLNS–BNKT ceramics at 60 °C for 30 min and 35 kV/cm, piezoelectric parameters such as k_p and d_{33} were determined through the piezoelectric resonance method obtained by an impedance analyzer and d_{33} meter (YE2730A, Sinocera), respectively.

3 Results and discussion

3.1 Characteristics of $NaNbO_3$ templates

Figure 1b depicts the structure and microstructure of $Bi_{2.5}Na_{3.5}Nb_5O_{18}$ (BiNN5) precursor particles calcined at 1050 °C for 2.5 h. As observed in the inset of Fig. 1b, the BiNN5 precursor particle has a single-phase structure, and the diffraction peaks exhibit a bismuth layer structure, which is consistent with its microstructure. Notably, the intensity of the (*00 h*) peaks that characterize the orientation of BiNN5 particles is high, whereas the intensity of the (*hkl*) peaks is lower. Furthermore, Fig. 1b depicts that BiNN5 particles have a morphology characterized by a width of 2–5 μm, a length of 3–10 μm, and a thickness of 0.5–1 μm. This structure facilitates BiNN5 to have a considerably faster grain growth rate along the *b*-axis than along the *c*-axis. Hence, it is easy to produce large-sized, platelet-like morphology, which is the basis for synthesizing $NaNbO_3$ templates, similar to those reported by Li et al. [12].

Figure 1c depicts the microstructure and EDS spectrum of the $NaNbO_3$ templates calcined at 1000 °C for 2 h. The figure reveals the formation of a plate-like particle characterized by a width of 2–7 μm, a length of 5–12 μm, and a thickness of nearly 1 μm. Notably, this shape is beneficial for the synthesis of oriented KNN-based ceramics using $NaNbO_3$ templates. As they can be easily adjusted parallel to the rolling direction during the lamination process, the resulting ceramic structure can be highly oriented by rolling using $NaNbO_3$ templates.

A thorough observation of the EDS spectrum of $NaNbO_3$ material reveals the peaks corresponding to the elements Nb (2.17 keV), Na (1.03 keV), and O (1.5 keV). Nevertheless, the Bi peak does not appear, implying the complete transformation of BiNN5

particles into $NaNbO_3$ perovskite, which is consistent with the structural analysis findings depicted in Fig. 1d. According to Li et al. [12], the transition from a layer structure to a perovskite structure involves the diffusion of Na^+, K^+, and Bi^{3+} in the layers $[Bi_{2.5}Na_{3.5}Nb_5O_{16}]^{2-}$ (BiNN5) and the change of $(Bi_2O_2)^{2+}$ fluorite layers to the perovskite structure through topochemical conversion(see Fig. 3). Figure 1d shows the formation of a perovskite single-phase structure of $NaNbO_3$ templates. The high peak intensity indicates good crystallization, thereby verifying the complete transformation of BiNN5 particles into $NaNbO_3$ perovskite particles. In other words, the layered structure of $Bi_{2.5}Na_{3.5}Nb_5O_{18}$ can be converted to the perovskite structure of $NaNbO_3$, while maintaining the platelet particle morphology of $Bi_{2.5}Na_{3.5}Nb_5O_{18}$ [12].

Figure 4 depicts 2D and 3D-electron density maps in the unit cell of the $NaNbO_3$ template along < 200 > and < 100 > planes. The electron density distributions and chemical bonding nature between Na, Nb, and O atoms of the $NaNbO_3$ template are shown in Fig. 4. It can be observed in this figure that the charge density around Nb and Na atoms connected with humps is directed toward their neighboring O atoms similar to the research of Li et al. [13]. In other words, the outer-shell 4*d* and 3 *s* states electrons of Nb and Na atoms move to the 2*p* states of nearest neighbor O atoms, which obtains that the bonding behavior between the Nb–O and Na–O atoms is the ionic nature. Furthermore, according to electronegativity theory, the electronegativity values of Na, Nb, and O elements are 0.93, 1.6, and 3.44, respectively. Due to the electronegativity difference between Nb

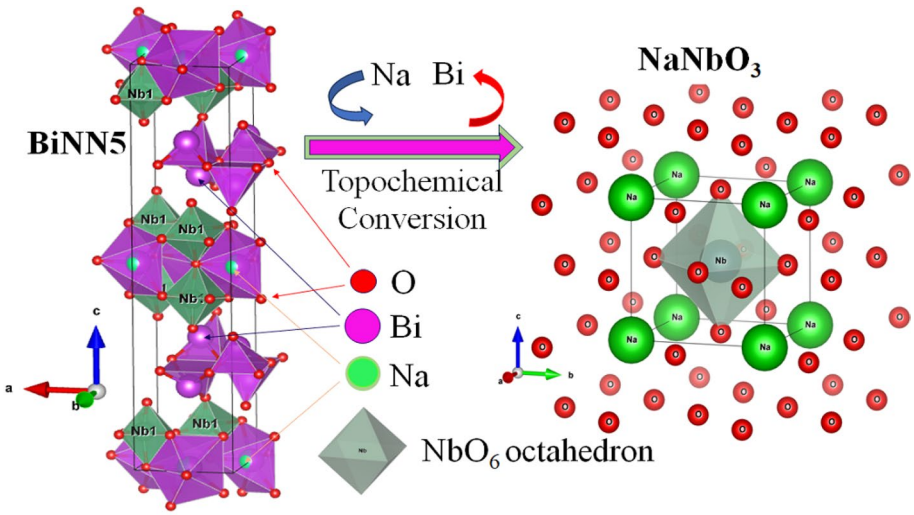

Fig. 3 Formation mechanism of $NaNbO_3$ templates

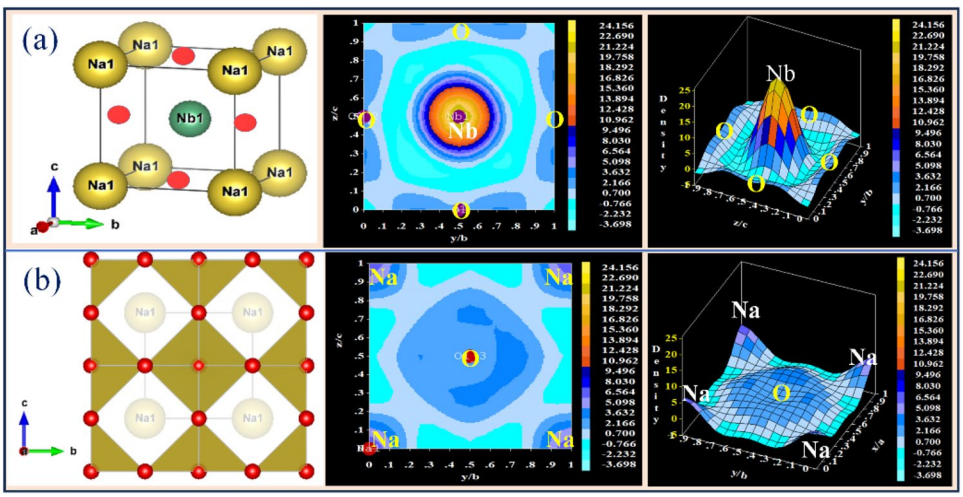

Fig. 4 The 2D and 3D-Fourier electron densities distribution of Na/Nb and O atoms on the yz plane ($x = 0$) in the unit cell of the $NaNbO_3$ template on: **a** (200) and **b** (100) planes

and O, Na and O all greater than 1.7 lead to ionic bonding of Nb–O and Na–O [14]. The strong orbital hybridization between Nb 4d and Na 3 s and O 2*p* results in a high polarization, which also contributes to the improvement in the properties of materials [15].

3.2 Characteristics of KNLNS-BNKT synthesized by different methods

Figure 2 illustrates the process followed for the synthesis of random and oriented KNLNS–BNKT ceramics. As depicted in Fig. 2(b), textured $0.98(K_{0.48}Na_{0.48}Li_{0.04})(Nb_{0.95}Sb_{0.05})O_3 - 0.02Bi_{0.5}(Na_{0.4}K_{0.1})TiO_3$ ceramics with 3 mol% $NaNbO_3$ templates were fabricated through the casting technique. According to previous studies, the use of $NaNbO_3$ templates in the range of 1–10 wt% is suitable for distribution in the powder matrix, thereby promoting grain growth according to the template [16]. In our opinion, while the use of large $NaNbO_3$ molds can potentially improve the texture level, it can increase the risk of the formation of voids and other defects in the ceramic sample. Therefore, in this study, the $NaNbO_3$ orientation template content of 3 mol% was chosen, which is similar to that reported by Gao et al. [17]. As shown in Table 1, textured ceramics demonstrate lowered ceramic densities compared to their non-textured counterparts ($\rho_{Texture} = 4.48$ g/cm^3, $\rho_{Random} = 4.51$ g/cm^3). This agrees with the microstructure, wherein the textured ceramics have loose structures and larger pores, resulting in lower densities compared to non-textured ceramics. Notably, grain growth cannot eliminate the pores originating from the volatility of K and Na or the evaporation of binding substances during sintering [12]. The dielectric constant of textured ceramic is 1223 at room temperature which is higher compared to that of random ceramic ($\varepsilon_r = 1153$). Besides, the dielectric loss of ceramics tends to develop in the opposite direction ($Tan\delta_{Texture} = 0.045$, $Tan\delta_{Random} = 0.051$). This enhancement in the dielectric property can be attributed to the crystallographic grain orientation of the textured sample, as suggested by Li et al. [12].

As depicted in Fig. 5a, b, the structural and orientation characteristics are compared by measuring the X-ray diffraction (XRD) spectra of random and textured KNLNS-BNKT ceramics at $2\theta = 20–60°$. It is noted that all ceramic samples have a pure perovskite phase with an orthorhombic phase without a secondary phase. However, differences in intensity and peak position are observed between random and oriented ceramics. Specifically, in random KNLNS–BNKT ceramics, the (110) peak exhibits maximum intensity at $2\theta = 31.84°$. Meanwhile, in textured samples, intensities of (00 *l*) peaks at $2\theta = 22.25$ $(100)_O$; $2\theta = 45.41$ $(200)_O$; and $2\theta = 46.10$ $(002)_O$ can be observed, implying a strong < 001 > orientation of textured KNLNS–BNKTceramics. According to Gao et al. [17], 3% mole $NaNbO_3$ templates are effective in facilitating crystal orientation of textured KNNS-based ceramics along the < 001 > direction, which is confirmed by the presence of (00 *l*) diffraction peaks. This aligns with the microstructural analysis obtained from the SEM images of the ceramics, as shown in Fig. 5(c, d). Besides, the texturing degrees f(*00 l*) of KNLNS-BNKT ceramics were calculated using Lotgering's method [11] in Eq. (2) from the diffraction peaks in the 2θ range from 20° to 60°, which yields a value of 82% as listed in Table 1. As indicated in Fig. 5(d), the textured KNLNS-BNKT ceramics exhibit a larger grain size and more orderly arrangement, implying potential benefits to the electromechanical properties due to the crystal orientation effect. This will be discussed in the following sections.

To further characterize the elemental distributions in the ceramics, the chemical composition of the sintered KNLNS–BNKT ceramic was determined through EDS (Fig. 6a). The result implies a homogeneous distribution of all elements, which include Bi, O, Na, Ti, Nb, K, and Sb, in the samples, as presented in Fig. 6c–k. This confirms the successful diffusion of BNKT in the KNLNS lattice, which is similar to the

Table 1 Comparison of physical dielectric parameters of the KNLNS–BNKT ceramics with different fabrication methods

Samples	Density (g/cm^3)	ε_r	k_p	d_{33} (pC/N)	P_r (μC/cm^2)	E_c (kV/cm)	S_{max} (%)	d_{33}* (pm/V)	Texturing degrees (%)
Random ceramic	4.51	1153	0.36	210	12.5	7.8	0.13	325	0
Textured ceramic	4.48	1223	0.40	245	13.7	8.2	0.15	367	82

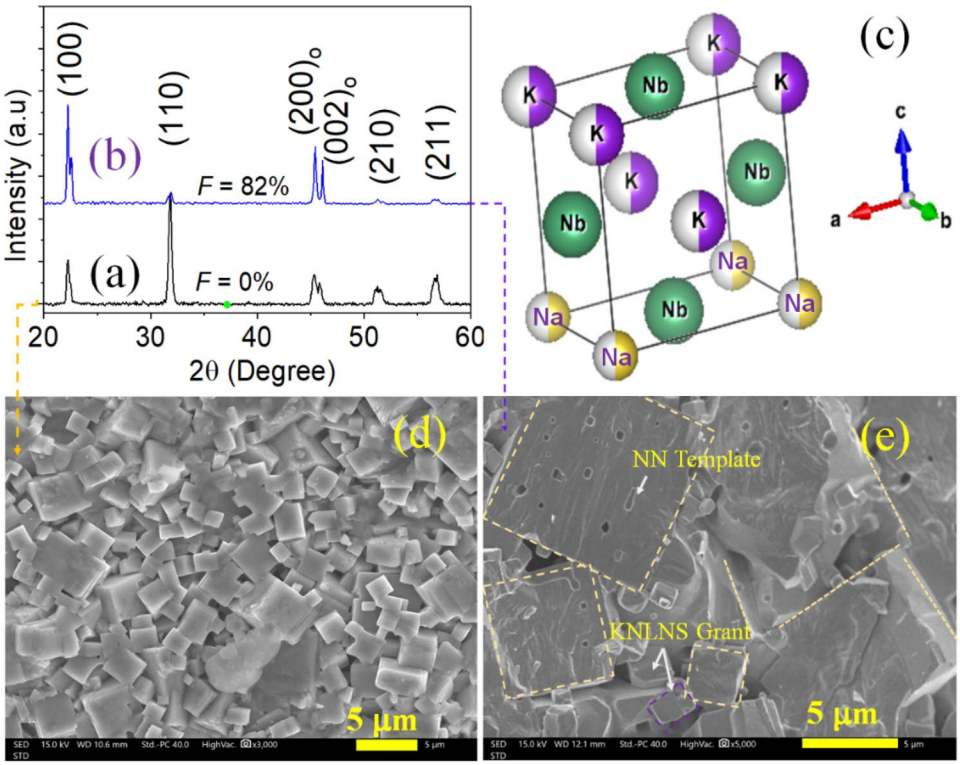

Fig. 5 XRD patterns of the (**a**) random and (**b**) oriented ceramics; (**c**) Crystal structure of perovskite-type KNN; Microstructure of (**d**) random and (**e**) oriented ceramics

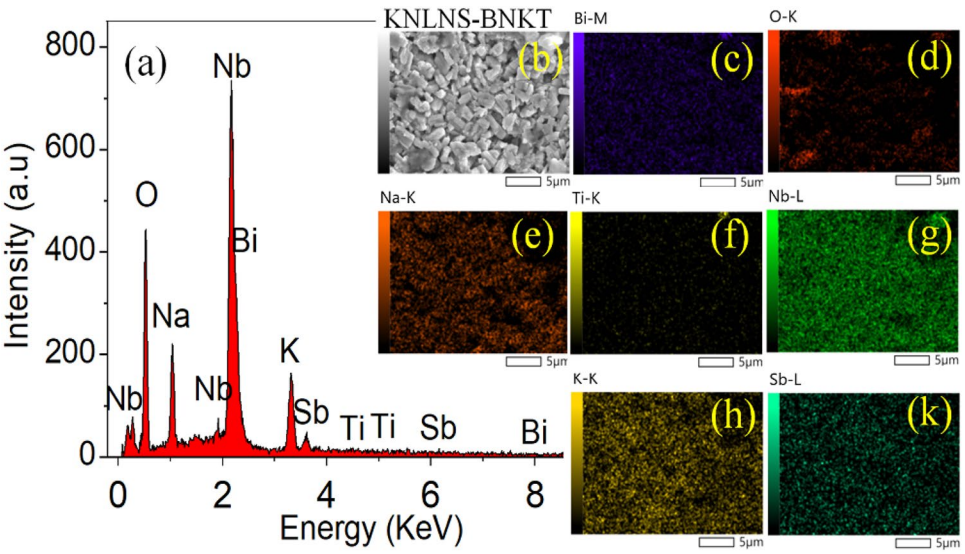

Fig. 6 **a** EDS analysis, **b** SEM image, and (**c**–**k**) element mappings of textured KNLNS–BNKT ceramics: **c** Bi, **d** O, **e** Na, **f** Ti, **g** Nb, **h** K, and **k** Sb

findings reported by Chen et al. [18]. However, the absence of lithium (Li) in Fig. 6 can be attributed to the low number and concentration being extremely low to be detected through the EDS spectroscopy method.

Recently, Raman spectroscopy has emerged as an effective tool for analyzing the crystalline structure and the phase transition of ceramics. Figure 7 depicts the Raman spectra of random and oriented KNLNS-BNKT ceramics at different measuring temperatures in the range of 30–300 °C. As illustrated in Fig. 7a, b, the majority of the Raman active modes of random and textured KNLNS–BNKT ceramics exhibit modes that are characteristic of KNN-based ceramics, with stretching modes corresponding to ν_1 and ν_2, while ν_5 represents the bending mode of the NbO_6 octahedra [19]. The peaks exhibit a pattern of shifting

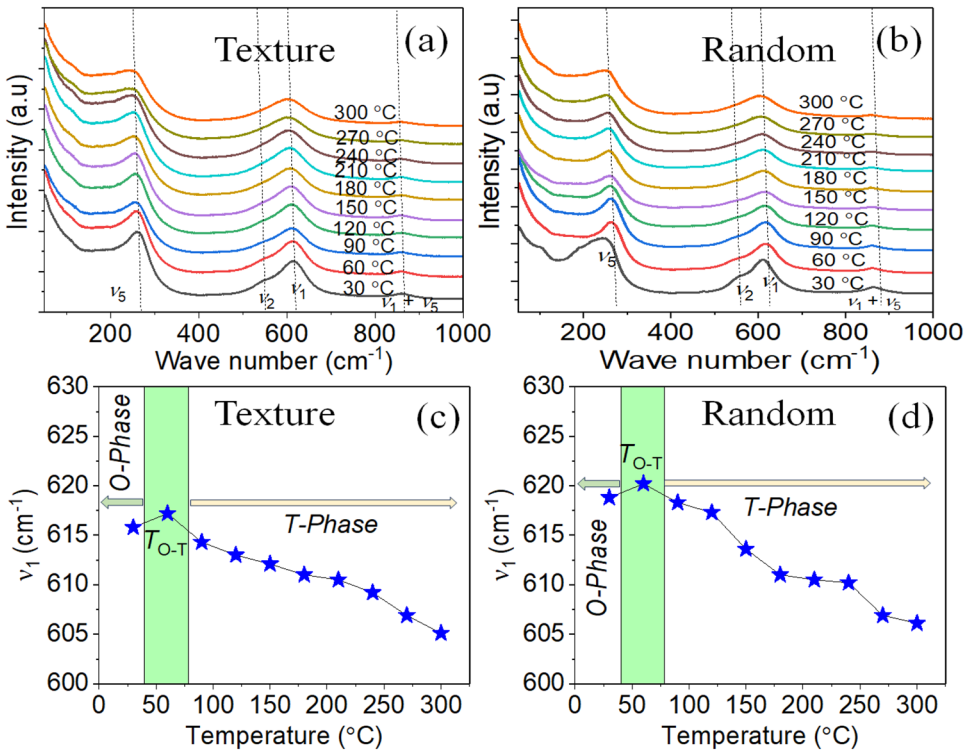

Fig. 7 In situ temperature dependence of Raman spectra: (**a**, **b**) Raman active modes and (**c**, **d**) shift of the ν_1 peak of random and textured ceramics in the range of 30–300 °C

to a lower wave number as the sample measurement temperature increases; this observation is similar to the report by Wang et al. [19]. In the aforementioned modes, the strong ν_1 mode localized around 600 cm^{-1} is said to be sensitive to phase transitions that are related to the double-degenerated symmetric O–Nb–O stretching vibration in the NbO_6 octahedron of KNN-based ceramics. In addition, a strong scattering peak is observed around 110 cm^{-1}, which is associated with the A-site vibrations in the ABO_3 (Fig. 5c) perovskite structure of the Na–O, K–O, Li–O, and Bi–O bonds [20]. Specifically, the ν_1 mode shifted to a lower wave number and exhibited broadening, accompanied by a gradual fading and disappearance of the ν_2 peak (Fig. 7(a)) as evidence of sensitivity to phase transitions in KNLNS–BNKT ceramics. This change is expected to result from a change in binding strength caused by the variation in the distance between B-site ions and their coordinated oxygen. Furthermore, Fig. 7c, d demonstrates that the temperature dependence of the ν_1 mode of ceramics ranges from 30 to 300 °C, displaying an abnormal point corresponding to the orthorhombic (*O*) and tetragonal (*T*) phase transition at ~ 50 °C ($T_{O–T}$). According to previous references [3, 5], the addition of Li^+, Sb^{5+}, and $Bi_{0.5}(Na_{0.4}K_{0.1})TiO_3$ to the KNN-based ceramics led to a decrease in the $T_{O–T}$ and increased the $T_{R–O}$ to room temperature simultaneously. This is almost consistent with the research results of dielectric properties of ceramics by determining the ε–T curves (Fig. 8). The origin of this dielectric anomaly at $T_{O–T}$ is mainly thought to be related to the change in ferroelectricity. According to Qi et al. [1], the change in vibration models is caused by the change of polarization configuration and oxygen octahedron tilt features with measuring temperatures. Raman spectroscopy results show that the shape and number of peaks remain unaltered, contributing to the thermally stable electrical properties of the KNLNS–BNKT ceramics in the research range of 30–300 °C. In general, the phase transition behavior of KNLNS–BNKT ceramics was confirmed through the Raman spectra analysis techniques. In other words, the orthorhombic (*O*) tetragonal (*T*) phase boundary is firmly proved by temperature-dependent Raman spectra [21].

As depicted in Fig. 8, we analyzed the dielectric properties of random and oriented KNLNS–BNKT ceramics to confirm that phase evolution is a function of temperature. As observed in this figure, three peaks appear at temperatures of nearly 345 °C, ~ 50 °C, and ~ 0 °C, which correspond to the phase transition temperatures of T_C, $T_{O–T}$, and $T_{R–O}$, respectively. It is well known that when the temperature of the ceramic samples exceeds T_C, the material transitions to the

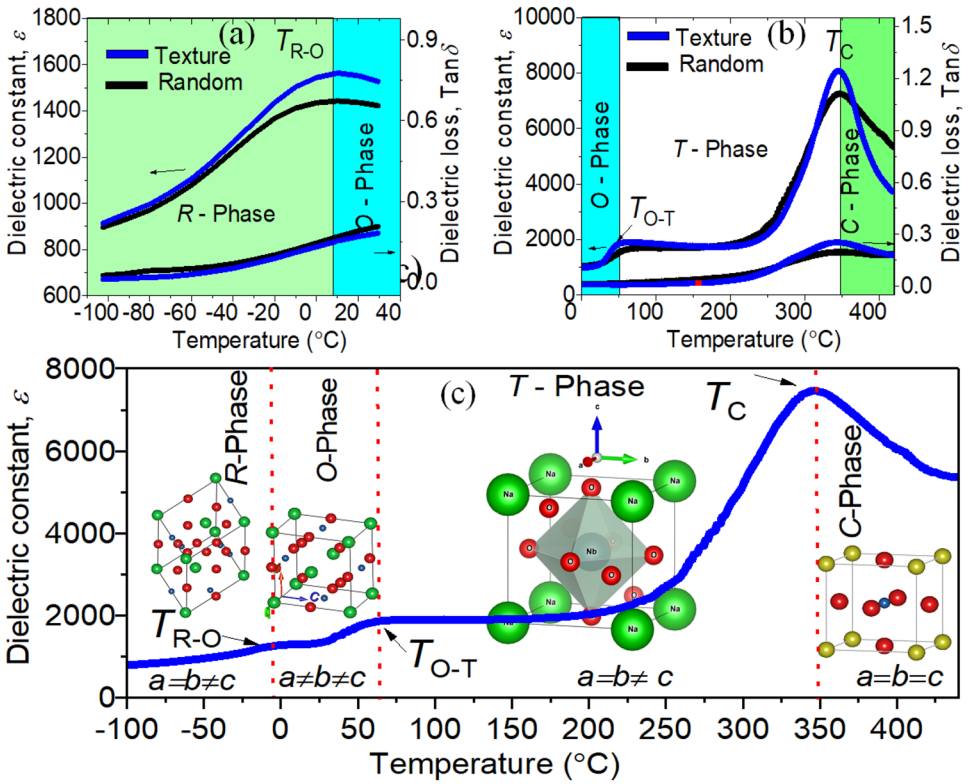

Fig. 8 Changes in the dielectric properties of random and oriented KNLNS–BNKT ceramics as a function of temperature

ceramic paraelectric phase, which affects its electrical properties, thereby necessitating its application at temperatures lower than T_C. In other words, if the working temperature of the sample is lower than T_C, the materials will transition into ferroelectric phases, facilitating possible applications. In general, the T_C, T_{O-T}, and T_{R-O} temperatures for pure KNN ceramics are approximately 420, 100, and −100 °C, respectively [18]. Herein, the doping of $Bi_{0.5}(Na_{0.4}K_{0.1})TiO_3$ helps in lowering the T_{O-T} temperature from 100 °C to ~ 46 °C and simultaneously increasing the T_{R-O} temperature from −100 °C to ~ 0 °C compared to the same structural transitions of KNN ceramics (see Fig. 8). This is due to the simultaneous substitution into the B-site (Ti^{4+}, Sb^{5+}, Nb^{5+}) and A-site (Na^+, K^+, Li^+, Bi^{3+}), resulting in a decrease in the T_{O-T} and a simultaneous increase in T_{R-O} to nearly room temperature while the T_C temperature undergoes a slight decrease (T_C = 346 °C). According to Garcia et al. [22], the strategy of utilizing simultaneous impurity pairs Li^+–Sb^{5+}, Li^+–Ta^{5+}, and Li^+–Sb^{5+}/Ta^{5+} is often employed because they have minimal impact on the Curie temperature (T_C). It is assumed that both random and oriented KNLNS-BNKT ceramics present the expected values with T_{O-T} = 56 °C, T_{R-O} = -5.9 °C, and T_{O-T} = 48, T_{R-O} = 3.7 °C, respectively, with phase boundary stabilizing near room temperature, resulting in improved piezoelectric properties in ceramics. The results reveal no significant change in the temperatures of T_C, T_{O-T}, and T_{R-O} in random and oriented KNLNS-BNKT ceramics, implying the complete interdiffusion of the NN templates into the matrix composition; this finding is similar to that reported by Li et al. [12]. Besides, the textured KNLNS-BNKT ceramics exhibited outstanding dielectric properties, achieving a dielectric maximum of 8021 at T_C, which is superior to those of random ceramics that have a value of 7280 at T_C. In short, the improved dielectric properties of textured ceramics are attributed to the preferential alignment in the (*h*00) direction with a larger number of 90 domains compared to non-textured ceramics [12]. This aligns with the significant improvement in the ferroelectric and piezoelectric properties observed in the oriented KNLNS–BNKT ceramic.

The piezoelectric parameters were determined from the resonance vibration spectrum of the random and oriented KNLNS–BNKT ceramics (Fig. 9a, b) and are listed in Table 1. The textured KNLNS–BNKT structural ceramic exhibits superior performance as its piezoelectric constant d_{33} of 245 pC/N is increased by 11.7%, whereas the electromechanical coupling coefficient k_p of 0.4 is increased by 11% as compared to those

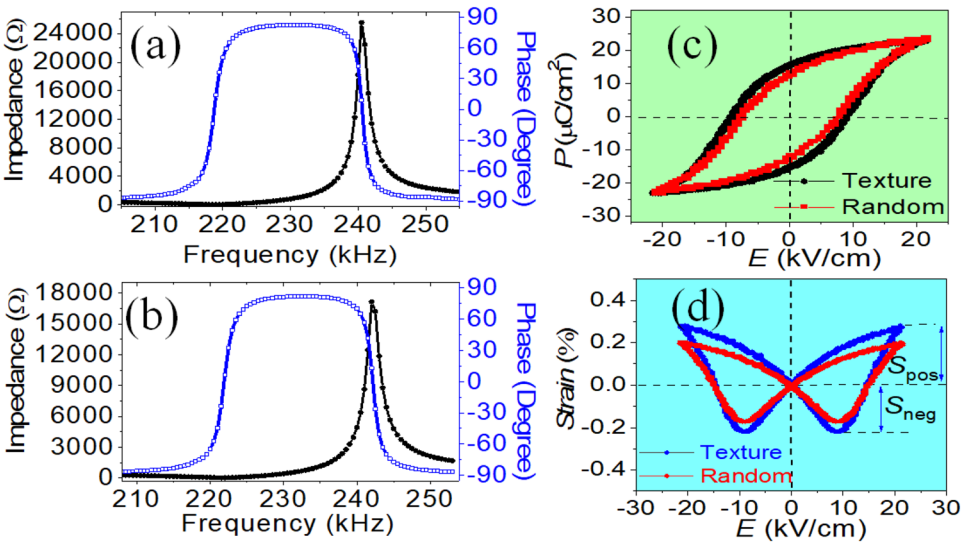

Fig. 9 **a, b** The resonance vibration spectra; **c** *P–E* hysteresis; and **d** *S–E* hysteresis loops of the random and oriented KNLNS–BNKT ceramics

of the random samples. The enhanced piezoelectric properties are attributed to increased orientation in ceramics. This implies that the enhancement in polarization is associated with the crystallographic grain orientation of the textured sample [23]. On the other hand, the textured ceramic not only exhibits superior piezoelectricity but also maintains a high T_C temperature, which sheds light on the application of oriented KNLNS–BNKT ceramics over a wide temperature range.

Figure 9c, d displays the *P–E* hysteresis and *S–E* hysteresis loops of the samples, all presenting the characteristic shape of ferroelectric materials. Besides, Table 1 reveals that the remnant polarization (P_r) of the oriented ceramic is 13.7 μC/cm^2 (increased by 9.6%), which is superior to that of random ceramics (12.5 μC/cm^2) and agrees with the research findings on piezoelectric characteristics. According to Li et al. [12], the high value of P_r of textured ceramic is attributed to the 90-domain contribution, which is in larger amounts compared to random ceramics. Furthermore, the high structural orientation in textured KNLNS–BNKT ceramics results in some domains with polar axes parallel to the electric field, thereby enabling their easy orientation according to the polarized electric field. Hence, the electrical properties are enhanced in a suitably oriented ceramic sample.

The maximum strain, S_{max} ($S_{max} = S_{pos} + S_{neg}$ [24]), and normalized strain, d_{33}* ($d_{33}^* = S_{max}/E_{max}$ [25, 26]), were determined from the butterfly-shaped strain curves of the random and oriented KNLNS–BNKT ceramics depicted in Fig. 9d. The parameters are listed in Table 1. Notably, the textured ceramics demonstrate a maximum strain of 0.15%, which is a larger value compared to non-textured ceramics (S_{max} = 0.13%). The textured ceramics exhibited high strain values, attributed to crystal orientation ceramics, with a contribution of 90 domains to the overall strain, which is larger than that of the non-textured ceramics and consistent with the previous studies [16]. Furthermore, as discussed earlier, the ferroelectricity of textured ceramics is higher than that of random ceramics, as evidenced by the remarkable values of maximum strain and normalized strain (d_{33}*). As presented in Table 1, textured ceramics exhibited a high d_{33}* value of 367 pm/V at *RT* (11.3% improvement compared to non-textured ceramic), which is probably attributed to the free energy flattening and energy barrier reduction in crystal orientation ceramics [24].

Figure 10a depicts the temperature-dependent *P–E* curve of the textured KNLNS–BNKT ceramics in the range of 20–230 °C. The calculated values of P_r and E_c are plotted in Fig. 10b. It is observed from the figure that the values of P_r and E_C increase initially with increasing temperature and reach the highest value (P_r = 15.3 μC/cm^2) at 50 °C (~ T_{O-T}), and the values decrease when further increasing temperature. As mentioned above, the ferroelectric phase transition occurred in the range of 40–60 °C. The phase transition within this temperature range led to an increase in polarization, yielding the highest P_r value at ~ 50 °C, which agrees with the previous reports [27]. It is well known that phase transition occurs with increasing temperatures, resulting in increased mobility of the

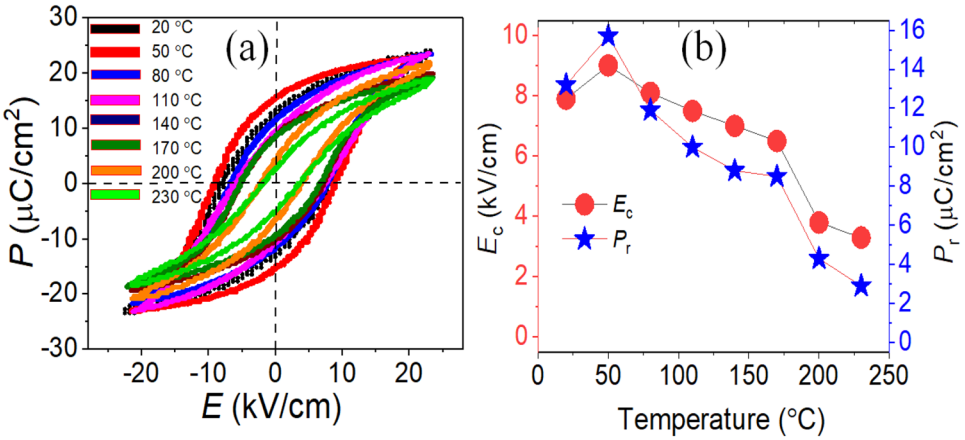

Fig. 10 **a** P–E hysteresis loops; **b** the calculated P_r and E_c values of the textured KNLNS–BNKT ceramics in different temperatures

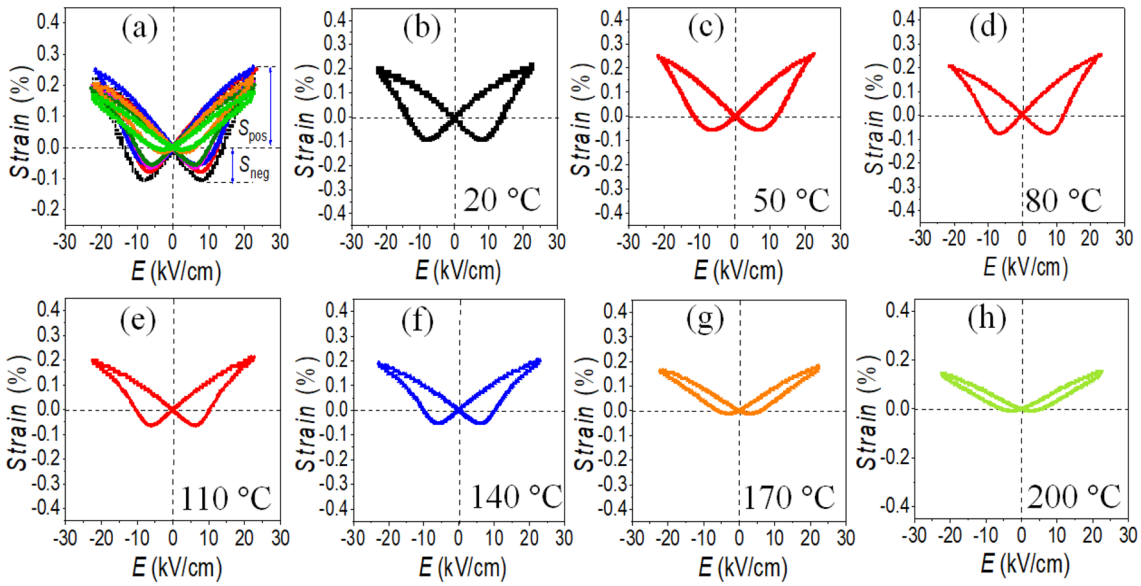

Fig. 11 **a** *S*–*E* hysteresis loops of the textured KNLNS-BNKT ceramics in different temperatures

domains and increased residual polarization. Nevertheless, once the high temperature exceeds T_{O-T}, the sample loses the *O*–*T* phase boundary effect, and the influence of thermal disturbance prevails, resulting in decreased polarization [28]. As shown in Fig. 10b, P_r at 230 °C is 3.2 μC/cm^2, demonstrating the excellent temperature stability of the textured KNLNS–BNKT ceramics in this study. These findings are valuable for practical applications.

Figure 11 depicts the strain response of textured ceramics at different temperatures. Figure 12 displays the variation in the values of S_{pos}, S_{neg}, and d_{33}* of the textured KNLNS–BNKT ceramics. The figure reveals that KNLNS–BNKT ceramic achieved the highest d_{33}* value of 495 pm/V at 50 °C. Notably, S_{max} (S_{pos} + S_{neg})

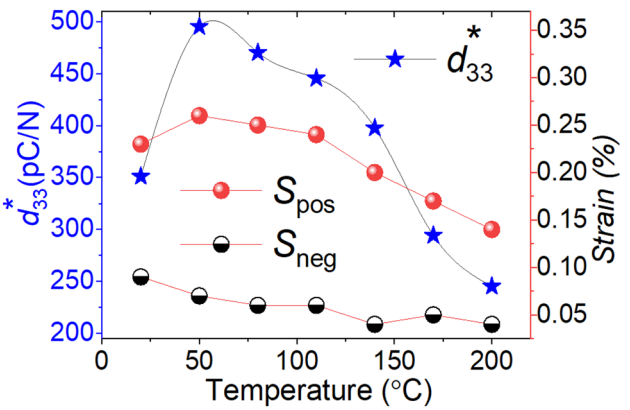

Fig. 12 Variation in positive strain (S_{pos}), negative strain (S_{neg}), and normalized strain (d_{33}*) with temperature of the textured KNLNS–BNKT ceramics

gradually increased with increasing temperature, leading to an increase in d_{33}* according to the following formula: $d_{33}^* = S_{max}/E_{max}$ [25, 26]. This finding demonstrates that the d_{33}* value in the *O–T* phase boundary achieved its highest value (d_{33}^* = 495 pm/V) at 50 °C around T_{O-T} (T_{O-T} = 46 °C). This is primarily attributed to the different variations between P_{max} and $P_{r,}$ which also contribute to the improvement in the temperature stability of strain and reverse piezoelectric properties, similar to that reported by Zhao et al. [28]. Besides, Fig. 12 shows that the d_{33}* value at 230 °C was 245 pm/V, thereby demonstrating the applicability of the ceramics with high-temperature stability. Moreover, the inclusion of BNKT complexes and single complexes like Li and Sb, forming the domain structure composed of micron- and nano-domains, could further contribute to the excellent comprehensive electrical properties [29].

4 Conclusion

In conclusion, this study presents the successful fabrication of KNLNS–BNKT lead-free ceramics by employing traditional ceramic and template grain growth methods. According to the results, the textured KNLNS–BNKT ceramic with 82% grain orientation exhibits better dielectric, piezoelectric, and ferroelectric properties compared to the randomly fabricated ceramics (the ε_r of 1223, the P_r of 13.7 μC/cm^2, the d_{33} of 245 pC/N, and the k_p of 0.40 increase by 11.7, 8, 25, and 11%, respectively) because of its preferential alignment in the (*h00*) direction with contributions from a larger amount of 90 domains. Furthermore, the normalized strain (d_{33}*) achieved the maximum value of 495 pm/V at 50 °C under an electric field of 24 kV/cm. This is attributed to the strategy of shifting the T_{R-O} and T_{O-T} phase transitions to near *RT*, leading to the coexistence of *R–O–T* phase boundaries, which is assumed to be responsible for the improvement of their electrical properties. In short, the orientation technique effectively enhances the electrical properties of lead-free KNN-based ceramics and finds extensive implementation across a broad operating temperature range.

Author contributions

All authors contributed to the study concept and design including doing experiments as well as discussing writing the manuscript.

Funding

This research was funded by Ministry of Education and Training under grant number B2023-DHH-30 and Hue University under the Core Research Program, Grant No. NCTB.DHH.2024.08.

Data availability

The raw data supporting the conclusions of this article will be made available by the authors on reasonable request.

Declarations

Conflict of interest The authors declare that they have no conflict of interest.

References

1. H. Qi, G. Wang, Y. Zhang, D. Wang, H. Liu, S. Deng, R. Zuo, J. Chen, Acta Mater. **248**, 118778 (2023)
2. N. Van Thinh, T. Van Chuong, T.N. Dat, V.T. Tung, J. Ceram. Proc. Res. **24**, 478–485 (2023)
3. L.D. Vuong, N.Q. Lich, N.X. Cuong, V.Q. Nha, N.D. Nhat, L.D. Hieu, L.P. Son, H.T.T. Linh, N.H. Chuc, T.N.A. Tuyen, T.N. Dat, P.-C. Wei, Mater. Res. Express **10**, 105701 (2023)
4. P. Song, Z. Zhu, Z. Yao, H. Hao, M. Cao, H. Liu, J. Mater. Sci. Mater. Electron. **35**, 58 (2024)
5. L.D. Vuong, N.Q. Lich, V.Q. Nha, N.D. Nhat, N.H. Chuc, J. Mater. Sci. Mater. Electron. **34**, 1963 (2023)
6. S. Zhang, B. Malič, J.-F. Li, J. Rödel, J. Mater. Res. **36**, 985–995 (2021)
7. X. Feng, Y. Zhao, Y. Wang, Y. Xie, P. Han, Y. Li, X. Hao, Ceram. Int. **50**, 1788–1794 (2024)
8. P. Li, J. Zhai, B. Shen, S. Zhang, X. Li, F. Zhu, X. Zhang, Adv. Mater. **30**, 1705171 (2018)
9. Y. Saito, H. Takao, T. Tani, T. Nonoyama, K. Takatori, T. Homma, T. Nagaya, M. Nakamura, Nature **432**, 84–87 (2004)
10. L. Liu, Z. Guo, Y. Wang, J. Mater. Sci. Mater. Electron. **29**, 9635–9642 (2018)
11. F. Lotgering, J. Inorg. Nucl. Chem. **9**, 113–123 (1959)
12. L. Li, W. Bai, Y. Zhang, B. Shen, J. Zhai, J. Alloy. Compd. **622**, 137–142 (2015)

13. C. Li, L. Wang, Z. Wang, Y. Yang, W. Ren, G. Yang, Sci. Rep. **6**, 37788 (2016)
14. J. Mullay, in *Estimation of Atomic and Group Electronegativities*, Electronegativity, (Springer, 2005) pp. 1-25.
15. J. Tian, Y. Cao, K. Xu, M. Zhan, D. Zhang, H. Tian, B. Zhang, Y. Xu, Mater. Res. Bull. **169**, 112550 (2024)
16. A.B. Haugen, E. Ringgaard, F. Levassort, J. Phys. Mater. **4**, 044002 (2021)
17. S. Gao, P. Li, J. Qu, M. Sun, J. Hao, P. Fu, Z. Pan, J. Zhai, W. Li, J. Materiomics **9**, 261–268 (2023)
18. B. Chen, J. Ma, S. Wu, B. Wu, J. Mater. Sci. Mater. Electron. **28**, 3299–3308 (2017)
19. D. Wang, F. Hussain, A. Khesro, A. Feteira, Y. Tian, Q. Zhao, I.M. Reaney, J. Am. Ceram. Soc. **100**, 627–637 (2017)
20. L.D. Vuong, D.A. Quang, V.T. Tung, N.H. Chuc, N.N. Trac, J. Mater. Sci. Mater. Electron. **31**, 18056–18069 (2020)
21. X. Lv, J. Wu, J. Zhu, D. Xiao, Phys. Chem. Chem. Phys. **20**, 20149–20159 (2018)
22. J.E. Garcia, F. Rubio-Marcos, J. Appl. Phys. (2020). https://doi.org/10.1063/5.0002983
23. A. Hussain, M.-H. Kim, Piezoelectric Mater. (2016). https://doi.org/10.5772/62688
24. B. He, Y. Du, Y. Liu, J. Wang, W. Liu, H. Xu, J. Mater. Sci. Mater. Electron. **32**, 18240–18250 (2021)
25. Z. Cen, M. Feng, F. Cao, Y. Jiang, Z. Xu, C. Zhou, K. Wang, N. Luo, J. Materiomics (2023). https://doi.org/10.1016/j.jmat.2023.11.018
26. J.-S. Lee, K.-N. Pham, H.-S. Han, H.-B. Lee, V.D.N. Tran, J. Korean Phys. Soc. **60**, 212–215 (2012)
27. Y. Tang, L. Wang, W. Ren, Y. Quan, J. Zhao, Z. Wang, K. Zheng, J. Zhuang, G. Niu, Crystals **12**, 1784 (2022)
28. C. Zhao, J. Yin, Y. Huang, J. Wu, Dalton Trans. **48**, 11250–11258 (2019)
29. H. Li, N. Chen, J. Xing, H. Chen, Z. Tan, M. Mo, Q. Chen, J. Zhu, F. Li, Z. Liu, W. Ouyang, H. Zhu, J. Mater. Chem. C **12**, 1809–1819 (2024)

Terms and Conditions

Springer Nature journal content, brought to you courtesy of Springer Nature Customer Service Center GmbH (“Springer Nature”).
Springer Nature supports a reasonable amount of sharing of research papers by authors, subscribers and authorised users (“Users”), for small-scale personal, non-commercial use provided that all copyright, trade and service marks and other proprietary notices are maintained. By accessing, sharing, receiving or otherwise using the Springer Nature journal content you agree to these terms of use (“Terms”). For these purposes, Springer Nature considers academic use (by researchers and students) to be non-commercial.
These Terms are supplementary and will apply in addition to any applicable website terms and conditions, a relevant site licence or a personal subscription. These Terms will prevail over any conflict or ambiguity with regards to the relevant terms, a site licence or a personal subscription (to the extent of the conflict or ambiguity only). For Creative Commons-licensed articles, the terms of the Creative Commons license used will apply.
We collect and use personal data to provide access to the Springer Nature journal content. We may also use these personal data internally within ResearchGate and Springer Nature and as agreed share it, in an anonymised way, for purposes of tracking, analysis and reporting. We will not otherwise disclose your personal data outside the ResearchGate or the Springer Nature group of companies unless we have your permission as detailed in the Privacy Policy.
While Users may use the Springer Nature journal content for small scale, personal non-commercial use, it is important to note that Users may not:

1. use such content for the purpose of providing other users with access on a regular or large scale basis or as a means to circumvent access control;
2. use such content where to do so would be considered a criminal or statutory offence in any jurisdiction, or gives rise to civil liability, or is otherwise unlawful;
3. falsely or misleadingly imply or suggest endorsement, approval , sponsorship, or association unless explicitly agreed to by Springer Nature in writing;
4. use bots or other automated methods to access the content or redirect messages
5. override any security feature or exclusionary protocol; or
6. share the content in order to create substitute for Springer Nature products or services or a systematic database of Springer Nature journal content.

In line with the restriction against commercial use, Springer Nature does not permit the creation of a product or service that creates revenue, royalties, rent or income from our content or its inclusion as part of a paid for service or for other commercial gain. Springer Nature journal content cannot be used for inter-library loans and librarians may not upload Springer Nature journal content on a large scale into their, or any other, institutional repository.
These terms of use are reviewed regularly and may be amended at any time. Springer Nature is not obligated to publish any information or content on this website and may remove it or features or functionality at our sole discretion, at any time with or without notice. Springer Nature may revoke this licence to you at any time and remove access to any copies of the Springer Nature journal content which have been saved.
To the fullest extent permitted by law, Springer Nature makes no warranties, representations or guarantees to Users, either express or implied with respect to the Springer nature journal content and all parties disclaim and waive any implied warranties or warranties imposed by law, including merchantability or fitness for any particular purpose.
Please note that these rights do not automatically extend to content, data or other material published by Springer Nature that may be licensed from third parties.
If you would like to use or distribute our Springer Nature journal content to a wider audience or on a regular basis or in any other manner not expressly permitted by these Terms, please contact Springer Nature at

onlineservice@springernature.com